

Experimental Investigation of Composite Circular Encased GFRP I-Section Concrete Columns under Different Load Conditions

Hiba Shihab Ahmed

Department of Civil Engineering, College of Engineering, University of Baghdad, Baghdad, Iraq
heba.ahmed2201M@coeng.uobaghdad.edu.iq (corresponding author)

Abbas Allawi

Department of Civil Engineering, College of Engineering, University of Baghdad, Baghdad, Iraq
a.allawi@coeng.uobaghdad.edu.iq

Riyadh Hindi

Department of Civil Engineering, Saint Louis University, St. Louis, MO, USA
riyadh.hindi@slu.edu

Received: 26 July 2024 | Revised: 14 August 2024 | Accepted: 22 August 2024

Licensed under a CC-BY 4.0 license | Copyright (c) by the authors | DOI: <https://doi.org/10.48084/etasr.8521>

ABSTRACT

Pultruded materials made of Fiber-Reinforced Polymer (FRP) come in a broad range of shapes, such as bars, I-sections, C-sections, etc. FRP materials are starting to compete with steel as structural materials owing to their great resistance, low self-weight, and cheap maintenance costs, especially in corrosive conditions. This study aims to evaluate the effectiveness of a novel concrete Composite Column (CC) using Encased I-Section (EIS) as a reinforcement in contrast to traditional steel bars by using Glass Fiber-Reinforced Polymer (GFRP) as I-section (CC-EIS) to evaluate the effectiveness of the hybrid columns which have been built by combining GFRP profiles with concrete columns. To achieve the aims of this study, nine circular columns with a diameter of 150 mm and a height of 1000 mm were cast with compression strength equal to 42.4 MPa at the test day. The research involved three different types of reinforcement: Hybrid circular columns with GFRP I-section and 1% reinforcement ratio of steel bars, Hybrid circular columns with steel I-section and 1% reinforcement ratio of steel bars (the cross-section area of the I-section was the same for GFRP and for steel), and a reference column without an I-section. This study investigates the ultimate capacity, axial and lateral deformation, and failure mode of the circular columns under different loading conditions: concentric, eccentric (with eccentricities of 25 mm), and flexural loading. The results showed that the ultimate capacity of the composite columns using either encased steel I-section or GFRP I-section was higher than the traditional columns under all loading conditions. The concentric tested specimens, with steel I-section and with GFRP I-section, exceeded the ultimate strength of the reference specimen by 8.9% and 2.9%, respectively. Specimens with steel I-section and GFRP I-section achieved 11.9% and 9.7% higher ultimate strength than the reference specimens under a compression load of 25 mm eccentricity. Specimens with steel I-section and the specimens with GFRP I-section achieved ultimate strengths of 114.3% and 36.6% under flexural loading testing.

Keywords-composite column; GFRP I-section; steel I-section; concentric load; eccentric load; flexural load

I. INTRODUCTION

Composite Columns (CCs) can be cost-effective and support high loads with a smaller cross-section than regular columns. High-rise buildings frequently use these CCs because thus the size of the building's columns can be minimized and the amount of floor area that can be used for occupancy can be increased. Furthermore, the CC improves the building's overall stiffness by providing high shear resistance against powerful earthquakes and other lateral stresses. Three types of CC

sections are utilized in high-rise construction: (a) Fully Encased Composite (FEC) column; (b) Partially Encased Composite (PEC) column; and (c) Concrete-Filled Tube (CFT) [1].

A recent research trend is to replace steel sections with GFRP sections that have particular properties, including light column weight that relieves structure dead load and eliminates steel corrosion-related issues. These materials are highly resistant to environmental influences, so they can be shaped into complicated shapes, and can be added to existing buildings

to strengthen or repair them. The limited application of these profiles in civil building makes design requirements for GFRP sections essential [2]. GFRP can support a more significant load per unit weight than steel or concrete because it has a higher strength-to-weight ratio [3]. Pultruded FRP members are preferred because of their high production rate, low labor cost, and minimal produced waste [4]. GFRP pultruded beams have several benefits, including high strength and stiffness, light weight, free formability, and high durability, even in hostile environments. Encasing a pultruded GFRP section in concrete also has several benefits, including significantly lowering the structure's weight and deformation, improving ductility, raising the structure's flexural stiffness and strength capacity, and preventing GFRP section buckling [5]. GFRP sections have been used in many structural elements, and much research has been found on the uses of GFRP I-section in composite beams in particular. Authors in [6] found that using GFRP I-section was recommended for bridge construction due to their improved flexural and compressive strengths as well as their improved resistance to corrosion. Authors in [7] found that composite materials such as pultruded GFRP showed superior performance in floors, bridge decks, and beams under static and impact loads when mixed with concrete. Authors in [8] investigated the experimental response of composite reinforced concrete with GFRP and steel I-sections under limited cycles of repeated load. Authors in [9] found that the encased GFRP beams could significantly reduce the residual behavior of the fire-damaged columns. On the other hand, authors in [10] found that the location of GFRP bars plays a crucial role. Optimal positioning is essential for enhanced fire resistance. Specifically, placing GFRP more centrally, and away from the ends, has a positive impact, resulting in superior fire resistance performance. Authors in [11] provided a sound foundation for the efficient use of concrete and GFRP composites. Authors in [12] reported that FRP materials despite their tensile stress endurance, their low cost and its lightweight nature, have found limited use. However, there have not been many studies about the Encased Concrete GFRP I-section CCs.

II. EXPERIMENTAL PROGRAM

A. Test Specimen Specifications

Nine circular reinforced concrete columns were constructed and were categorized into three types based on the use of an I-section. Three were composite-encased columns with steel I-sections in the center (IS), the others were composite columns with GFRP I-sections in the center (IG), and the last three were reference columns without an I-section (R). These specimens were fabricated, cast, and tested under concentric (E00), eccentric (E25), and flexural (F) loading.

All specimens had the same reinforcement, including six longitudinal steel bars Ø 6mm whereas spiral transfer reinforcement with a diameter of (4mm) was used with a spiral pitch of (50mm). For steel I-section and GFRP I-section, the cross-section area was the same and equal to (50x25x4) mm. All specimens had the same diamensions: 1000 mm height and 150 mm diameter. The column specimen details are shown in Figure 1 and Table I.

TABLE I. DETAILS OF TEST SPECIMENS

Group	Specimen	Type of I-section	Type of loading
G1	R-E00	w/o	Concentric
	IG-E00	GFRP	
	IS-E00	STEEL	
G2	R-E25	w/o	Eccentric with 25mm eccentricity
	IG-E25	GFRP	
	IS-E25	STEEL	
G3	R-F	w/o	Flexural
	IG-F	GFRP	
	IS-F	STEEL	

R: refers to columns without I-section, IS refers to I-section steel, IG refers to I-section GFRP, E00 refers to the concentric test, E25 refers to the eccentric test at 25 mm, F: refers to the flexural loading test

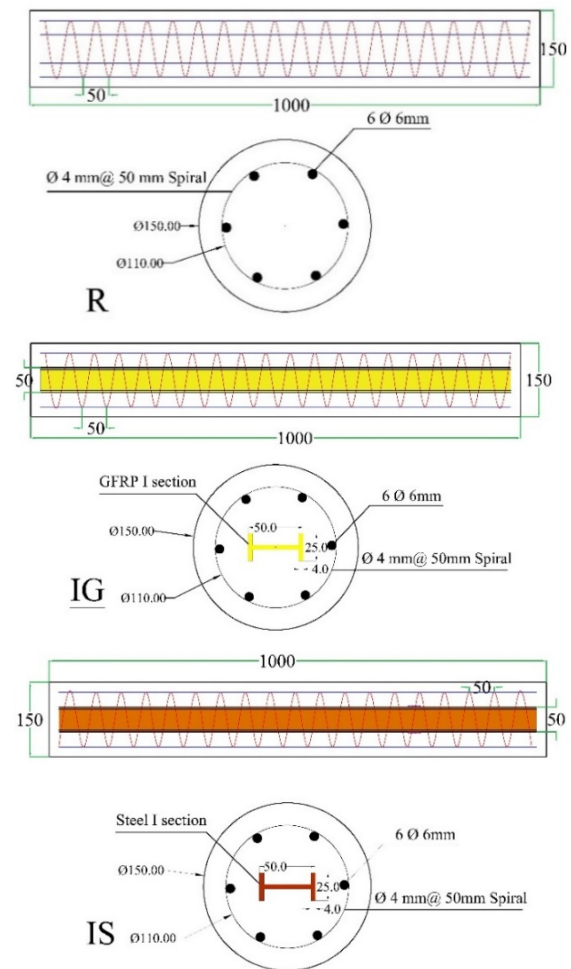


Fig. 1. Specimen details (all dimensions in mm).

B. Material Properties

1) Concrete

The study required making concrete of normal strength. It was cast using a central mixer. The mix design of cement, sand and gravel was 1:1.93:2.27 (by weight), respectively. At the testing day, the average compressive strength was 42.4 MPa. Table II lists the proportions of normal-strength concrete utilized in the concrete mix.

TABLE II. CONCRETE MIX PROPORTIONS

Mix proportion (kg/m ³)				
Cement	Gravel	Sand	Water	Additive type (HM99)
430	980	830	147	5

In order to cast the test specimens, the corresponding ASTM standards were considered [13-15] to estimate compressive strength, splitting tensile strength, and rupture modulus (Table III).

TABLE III. MECHANICAL PROPERTIES OF HARDENED CONCRETE

Compressive strength f'_c (MPa)	Splitting tensile strength f_{ct} (MPa)	Modulus of rupture R (MPa)
42.4	4.01	4.29

2) Steel

Three members with a length of 500 mm from each steel bar (Ø6mm and Ø4mm) were used. The steel used was of Ukrainian origin. Its mechanical properties are listed in Table IV.

TABLE IV. PHYSICAL-MECHANICAL PROPERTIES OF STEEL REINFORCEMENT

Diameter (mm)	Measured diameter (mm)	Cross-sectional area (mm ²)	Yield strength (MPa)	Tensile strength (MPa)	Elongation (%)
4	4.33	14.76	609	771	20
6	6	169.64	430	544.36	20

a) Steel I-Section Properties

I-section with dimensions 50×25×4 mm was required. Since this section is not available in the local markets, it was manufactured, and the steel plate thickness used was 4 mm, joined by welding wire. Tensile coupon tests of steel were also manufactured, and their dimensions followed [16]. The mechanical properties of steel plate testing met the requirements of [17, 18], as shown in Table V.

TABLE V. MECHANICAL PROPERTIES OF STEEL PLATES

Coupon	Thickness (mm)	Yield strength (MPa)	Ultimate strength (MPa)	Maximum elongation (%) in 50 mm
Steel plate	3.6	355.5	450.2	28

b) GFRP I-Section Properties

GFRP structural 50×25×4 mm I-sections were ordered from DURA Composites. Table VI shows the properties of GFRP as indicated in the inspection report provided by the supplier.

TABLE VI. MECHANICAL PROPERTIES OF GFRP

GFRP profile	Product size (mm)	Tensile strength (MPa)	Compressive strength (MPa)	Modulus of elasticity (MPa)
I-Beam	50×25×4	681.57	350	40410

C. Specifics of the Tested Specimen Setup

The column specimens were tested until they failed under loads through pinned end supports. CFRP sheets were used to reinforce the columns to prevent early failure caused by the applied load. Continuous 100 mm-wide CFRP strips and two types of bonding material were used at the top and bottom of each column specimen. The loading was applied using a 2000 kN load cell installed between the loading head and the hydraulic jack. To record the axial displacement of the specimens, two LVDTs were installed at the base and the top of the machine used for testing. The lateral displacement was measured using two other LVDTs placed on the left and right of the center of the specimens. Two rigid steel loading heads with 100 mm height and 15 mm thickness were fixed at the column ends before testing. During the testing period, all strain gauges were linked with an automatic data-acquiring system used to register the compressive load and all deformations caused by the load. The test setup and equipment are shown in Figure 2.

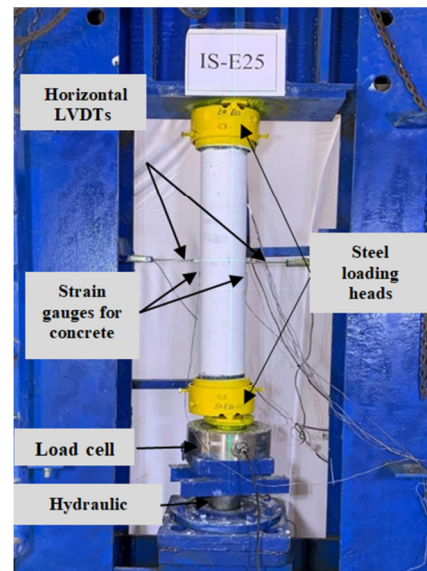


Fig. 2. Column specimen test setup.

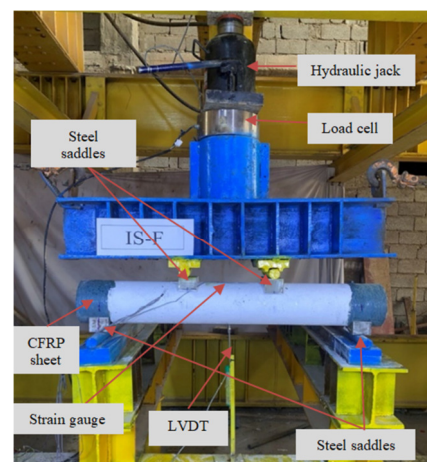


Fig. 3. Beam specimen test setup.

Four steel saddles were made to test a circular column as a beam, leading to an essential supported system. The beams were loaded with a roller support at one end and a pin support at the other. A 50-ton hydraulic jack and a 100-ton load cell were used to test the circular column under two-point loading. A single LVDT was used to measure the deflection at the mid-span, as illustrated in Figure 3. A computer system was used to gather the load and deformation data automatically.

III. TEST RESULTS

A. Load Capacity of CC-EIS Columns

The effect of CCs and I-section (steel or GFRP) columns on the ultimate strength of RC columns under several loading conditions are listed in Table VII. In the first group of concrete columns, which was tested under concentric load, the concentric tested specimens IS-E00 and IG-E00 achieved 8.9% and 2.9% ultimate strength higher than the reference specimen R-E00, respectively. Under a compression load of 25 mm eccentricity, specimens IS-E25 and IG-E25 achieved 11.9% and 9.7% higher ultimate strength than the reference specimen's. Under flexural loading test, specimens IS-F and IG-F reached 114.3% and 36.6% ultimate strength, respectively. Furthermore, as shown in Figure 4, under all loading conditions, the tested specimens with the same design parameters showed a reduction in ultimate strength when the steel I-section was replaced by the GFRP I-section.

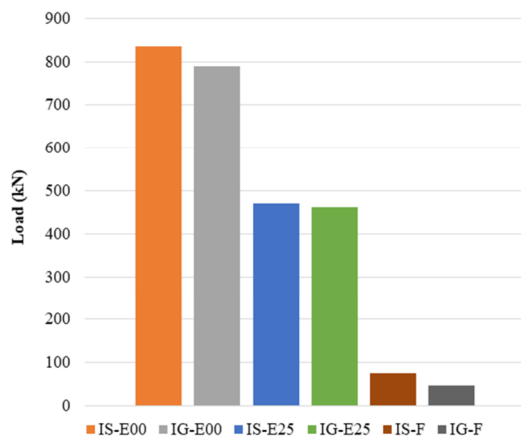


Fig. 4. Ultimate load capacity of IS and IG specimens under different load conditions.

TABLE VII. EXPERIMENTAL LOAD CAPACITY RESULTS

Group no.	Specimen ID	Ultimate load (kN)	$\frac{P_u (Exp.)}{P_u (Ref.)}$
G1	R-E00	766.7	Ref.
	IS-E00	835.4	1.09
	IG-E00	788.6	1.03
G2	R-E25	421.4	Ref.
	IS-E25	471.5	1.12
	IG-E25	462.4	1.1
G3	R-F	35	Ref.
	IS-F	75	2.14
	IG-F	47.8	1.36

For the concentric loading test, the ultimate strength of the specimen IG-E00 was less than about 5.9% of the ultimate

strength of the specimen IS-E00. Under a 25 mm eccentric load, the ultimate strength of IG-E25 was less by 1.96% than the specimen IS-E25's. The ultimate strength of the specimen IG-F was 56.9% less than the ultimate strength of the specimen IS-F under flexural load.

The results show that the ultimate strength and lateral deformation of concrete columns depend highly on the eccentricity of the applied load because the bending moment effect produces a tension zone and reduces the compression cross-sectional area, there is a drop in the capacity and an increase in lateral deformation.

B. Load-Deformation Curve of CC-EIS Columns

1) Load-Axial Displacement under Concentric Loading

Concerning the first group, the specimen R-E00 displayed an axial displacement of 1.67 mm and an axial capacity of 766.7 kN. The axial bearing capabilities of IS-E00 and IG-E00 were 835.4 kN and 788.6 kN, respectively, and the axial displacement slightly increased to 1.91 mm and 1.71 mm. The load-displacement responses for the group G1 specimens are displayed in Figures 5-7.

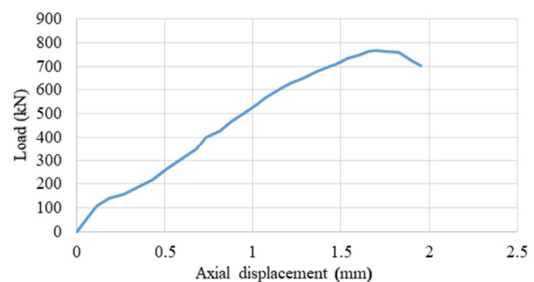


Fig. 5. Load-axial displacement response of R-E00 specimen.

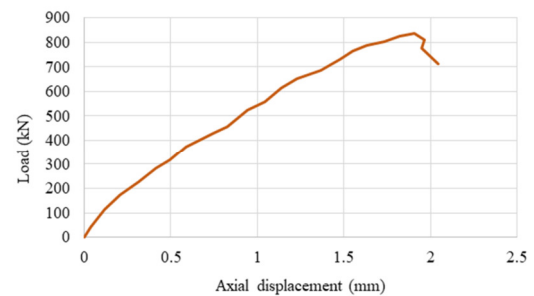


Fig. 6. Load-axial displacement response of IS-E00 specimen.

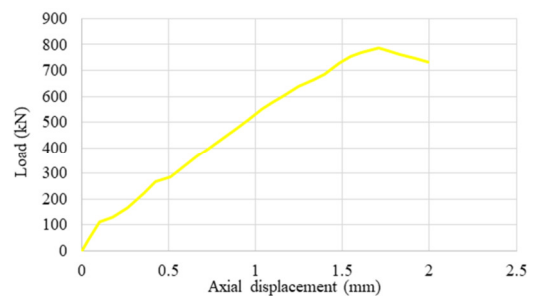


Fig. 7. Load-axial displacement response of IG-E00 specimen.

2) Load-Lateral Deformation under 25 mm Eccentric Loading

In the second group, the values of lateral deformation were close. It reached 3.61 mm, 3.23 mm, and 3.77 mm for specimens R-E25, IS-E25 and IG-25, respectively. The curves show a gradual upward growth when eccentric loading is applied. This behavior was also observed for columns evaluated under concentric load. Additionally, it should be noted that the concentrically loaded column reached ultimate load with a slight lateral displacement before failing. Columns subjected to eccentric loading, on the other hand, failed gradually as the lateral displacement increased. The ultimate load-lateral displacement of the examined specimens is displayed in Figures 8-10 for all specimens.

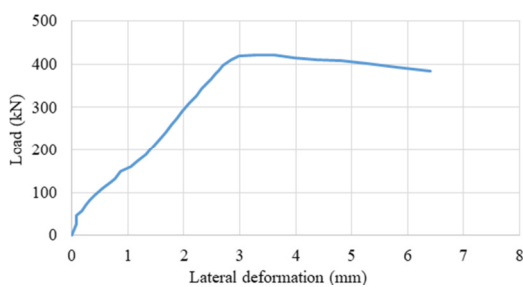


Fig. 8. Load-lateral deformation response of R-E25 specimen.

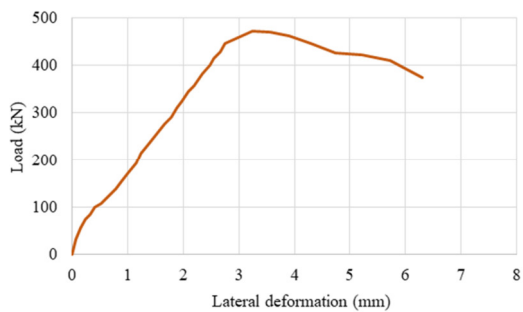


Fig. 9. Load-lateral deformation response of IS-E25 specimen.

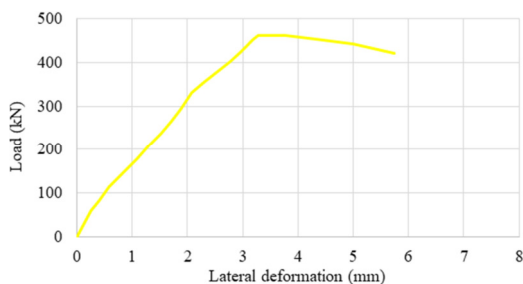


Fig. 10. Load-lateral deformation response of IG-E25 specimen.

3) Load-Deflection under Flexural Loading

The last group of specimens was tested as a beam. The experimental results of the beam specimens are shown in Figures 11-13. For all tested specimens, to ensure no bearing failure, a layer of CFRP wrap was wrapped around the specimen's 100 mm length on both ends. The mid-span deflection of the R-F specimen was recorded with a maximum

load of 35 kN achieved at a mid-span deflection of 5.96 mm. After the maximum load was reached for specimen R-F, the load was maintained until sudden failure occurred in the tension region of the beam specimen at a mid-span deflection of 6.77 mm. The specimen IS-F was the second tested. With a load of 75 kN at a mid-span deflection of 8.47 mm, this specimen achieved the highest maximum load of all the specimens. Specimen IG-F was tested last. This specimen reached a maximum load of 47.8 kN at a mid-span deflection of 11.8 mm.

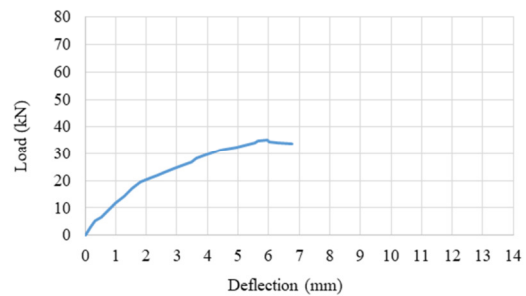


Fig. 11. Load-deflection curve of the R-F specimen.

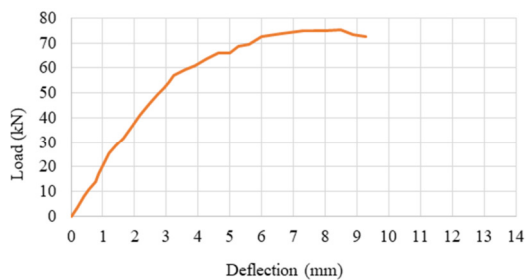


Fig. 12. Load-deflection curve of the IS-F specimen.

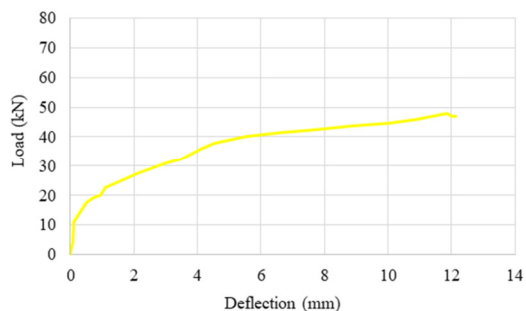





Fig. 13. Load-deflection curve of the IG-F specimen.




C. Modes of Failure

All column specimens were tested until failure. Depending on the kind of reinforcement, various failure modes were noted. At first, every specimen exhibited similar behavior. The specimen's top was where the cracks initially started to show. The cracks began expanding to all sides as the test continued. The sudden breaking of the concrete cover caused the load to decrease once the maximum load (P_{ult}) was reached. The failure mode of most experimental specimens was dominated by compression failure. Concrete cover spalling was observed at the mid-height of almost all tested columns due to the

successive increases of the applied loading, with buckling observed in steel bars and rupture in ties and the GFRP I-section.

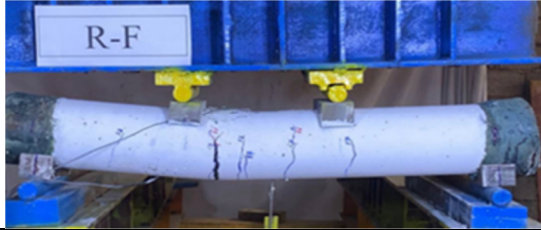
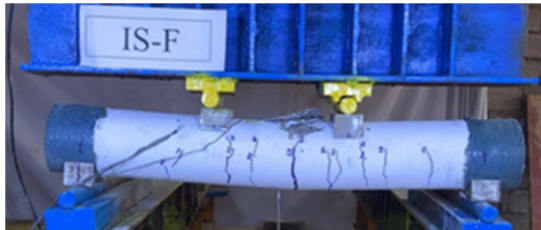
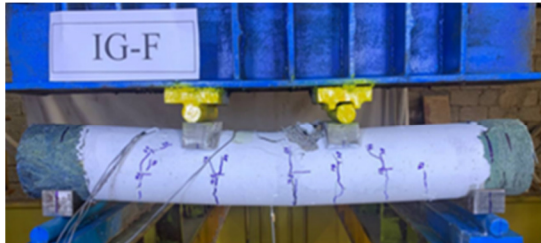
TABLE VIII. SPECIMENS TESTED AS COLUMNS

Specimen ID & type of loading	Tested specimen	Failure mode
R-E00 Concentric		Compression failure mode. Crush in the concrete cover. Buckling in the longitudinal steel bar. Ruptured in the spiral tie.
IS-E00 Concentric		Compression failure mode. Crush in the concrete cover in the compression zone. Buckling in the longitudinal steel bar. Ruptured in the spiral tie.
IG-E00 Concentric		Compression failure mode. Crush in the concrete cover in the compression zone. Ruptured in the GFRP I-section. Buckling in the longitudinal steel bar. Ruptured in the spiral tie.

R-E25 Eccentric		Crush in the concrete cover in the compression zone. Cracks in the tension zone. Buckling in the longitudinal steel bar.
IS-E25 Eccentric		Crush in the concrete cover in the compression zone. Cracks in the tension zone. Buckling in the longitudinal steel bar.
IG-E25 Eccentric		Crush in the concrete cover in the compression and tension zone. Buckling in the longitudinal steel bar. Ruptured in the GFRP I-section.

In all columns, the failure occurred at the section located at the mid-upper part of the tested specimens except the specimen IS-E00, in which the failure occurred at the section located at the mid-lower part. The failure modes for all tested column specimens are shown in Tables VIII and IX.

TABLE IX. SPECIMENS TESTED AS BEAMS

Specimen ID & Failure Mode
<p>R-F</p> <p>- Tensile failure mode.</p> <p>- Visible tension cracks at the specimen's mid-span and significant concrete crushing in the compression zone.</p> 
<p>IS-F</p> <p>- Tensile failure mode</p> <p>- Visible large tension cracks at the specimen's mid-span and significant concrete crushing in the compression zone.</p> 
<p>IG-F</p> <p>- Tensile failure mode</p> <p>- Visible large tension cracks at the specimen's mid-span and significant concrete crushing in the compression zone.</p> 

IV. CONCLUSION

This paper presents an experimental study of the behavior of composite circular concrete columns with encased GFRP I-section and steel I-section under different loading conditions. The following conclusions were derived from the experimental results:

1. The composite columns achieved higher loading capacity using steel or GFRP I-section than the control columns for all loading conditions.
2. Using the GFRP I-section increased the maximum load capacity of the column by 2.9% under concentric load, 9.7% under 25 mm eccentric load, and about 36.6% under flexural load.
3. Under concentric load, IS-E00 and IG-E00 specimens exceeded the ultimate strength of the reference specimen R-E25 by 8.9% and 2.9%, respectively.
4. With a 25 mm eccentric load, IS-E25 and IG-E25 specimens achieved 11.9% and 9.7% higher ultimate strength than the reference specimen R-E25.
5. Specimens IS-F and IG-F achieved ultimate strengths of 114.3% and 36.6% of the reference specimen's strength under flexural loading.
6. In composite columns, replacing steel I-section with GFRP I-section can decrease the ultimate strength of columns under concentric load by 5.9%. Under a 25 mm eccentric load, the composite column with GFRP I-section achieved an ultimate strength equal to 98% of the specimen's strength with steel I-section. This percentage decreased under flexural loading to 63.7%.
7. The ultimate strength and lateral deformation of columns are greatly affected by the eccentricity of the applied load, which results in a loss in specimen capacity and an increase in lateral deformation.

REFERENCES

- [1] T. Kartheek and T. Venkat Das, "3D modelling and analysis of encased steel-concrete composite column using ABAQUS," *Materials Today: Proceedings*, vol. 27, pp. 1545–1554, Jan. 2020, <https://doi.org/10.1016/j.matpr.2020.03.200>.
- [2] S. M. Swelem, M. L. El-Naggar, and M. A. Yousef, "Simulation of structural GFRP sections encased in concrete columns subjected to axial load," in *46th International Conference on Computers & Industrial Engineering*, Tianjin, China, Oct. 2016, pp. 1–8.
- [3] T. H. Ibrahim, I. A. S. Alshaarabaf, A. A. Allawi, N. K. Oukaili, A. El-Zohairy, and A. I. Said, "Theoretical Analysis of Composite RC Beams with Pultruded GFRP Beams subjected to Impact Loading," *Engineering, Technology & Applied Science Research*, vol. 13, no. 6, pp. 12097–12107, Dec. 2023, <https://doi.org/10.48084/etasr.6424>.
- [4] E. M. Mahmood, T. H. Ibrahim, A. A. Allawi, and A. El-Zohairy, "Experimental and Numerical Behavior of Encased Pultruded GFRP Beams under Elevated and Ambient Temperatures," *Fire*, vol. 6, no. 5, May 2023, Art. no. 212, <https://doi.org/10.3390/fire6050212>.
- [5] E. M. Mahmood, A. A. Allawi, and A. El-Zohairy, "Flexural Performance of Encased Pultruded GFRP I-Beam with High Strength Concrete under Static Loading," *Materials*, vol. 15, no. 13, Jan. 2022, Art. no. 4519, <https://doi.org/10.3390/ma15134519>.
- [6] T. H. Ibrahim, A. A. Allawi, and A. El-Zohairy, "Impact Behavior of Composite Reinforced Concrete Beams with Pultruded I-GFRP Beam," *Materials*, vol. 15, no. 2, Jan. 2022, Art. no. 441, <https://doi.org/10.3390/ma15020441>.
- [7] A. A. Allawi and S. I. Ali, "Flexural Behavior of Composite GFRP Pultruded I-Section Beams under Static and Impact Loading," *Civil Engineering Journal*, vol. 6, no. 11, pp. 2143–2158, Nov. 2020, <https://doi.org/10.28991/cej-2020-03091608>.
- [8] T. H. Ibrahim and A. A. Allawi, "The Response of Reinforced Concrete Composite Beams Reinforced with Pultruded GFRP to Repeated Loads," *Journal of Engineering*, vol. 29, no. 1, pp. 158–174, Jan. 2023, <https://doi.org/10.31026/j.eng.2023.01.10>.
- [9] E. M. Mahmood, A. A. Allawi, and A. El-Zohairy, "Analysis and Residual Behavior of Encased Pultruded GFRP I-Beam under Fire Loading," *Sustainability*, vol. 14, no. 20, Jan. 2022, Art. no. 13337, <https://doi.org/10.3390/su142013337>.
- [10] M. R. Rasheed and S. D. Mohammed, "Structural Behavior of Concrete One-Way Slab with Mixed Reinforcement of Steel and Glass Fiber Polymer Bars under Fire Exposure," *Engineering, Technology & Applied Science Research*, vol. 14, no. 2, pp. 13380–13387, Apr. 2024, <https://doi.org/10.48084/etasr.6795>.
- [11] M. I. Ali, A. A. Allawi, and A. El-Zohairy, "Flexural Behavior of Pultruded GFRP-Concrete Composite Beams Strengthened with GFRP

- Stiffeners," *Fibers*, vol. 12, no. 1, Jan. 2024, Art. no. 7, <https://doi.org/10.3390/fib12010007>.
- [12] M. Abdulkhalik and A. H. Al-Ahmed, "The Flexural Behavior of One-Way Concrete Bubbled Slabs Reinforced by GFRP-Bars with Embedded Steel I-Sections," *Engineering, Technology & Applied Science Research*, vol. 14, no. 4, pp. 15860–15870, Aug. 2024, <https://doi.org/10.48084/etasr.7680>.
- [13] *ASTM C39/C39M-15(2015), Standard Test Method For Compressive Strength Of Cylindrical Concrete Specimens*. West Conshohocken, PA, USA: ASTM International, 2015.
- [14] *ASTM C496/C496M-17(2017), Standard Test Method for Splitting Tensile Strength of Cylindrical Concrete Specimens*. West Conshohocken, PA, USA: ASTM International, 2017.
- [15] *ASTM C293/C293M-16(2016), Standard Test Method for Flexural Strength of Concrete (Using Simple Beam With Center-Point Loading)*. West Conshohocken, PA, USA: ASTM International, 2016..
- [16] *ASTM A370-17(2017), Standard Test Methods and Definitions for Mechanical Testing of Steel Products*. West Conshohocken, PA, USA: ASTM International, 2017.
- [17] *ASTM A529/A529M-01(2001), Standard Specification for High-Strength Carbon-Manganese Steel of Structural Quality*. West Conshohocken, PA, USA: ASTM International, 2001.
- [18] *ASTM A36/A36M-05(2005), Standard Specification For Carbon Structural Steel*. West Conshohocken, PA, USA: ASTM International, 2005.